PAPER

Unconventional deformation and sound absorption properties of anisotropic magnetorheological elastomers

IOP Publishing Smart Materials and Structures
Smart Mater. Struct. **30** (2021) 105022 (12pp) https://doi.org/10.1088/1361-665X/ac2027

Unconventional deformation and sound absorption properties of anisotropic magnetorheological elastomers

Chuanlin Sun, Yinduan Gao, Bochao Wang, Xufeng Cao, Shouhu Xuan* and Xinglong Gong*

CAS Key Laboratory of Mechanical Behavior and Design of Materials, CAS Center for Excellence in Complex System Mechanics, Department of Modern Mechanics, University of Science and Technology of China (USTC), Hefei, People's Republic of China

E-mail: xuansh@ustc.edu.cn and gongxl@ustc.edu.cn

Received 9 June 2021, revised 18 August 2021
Accepted for publication 22 August 2021
Published 2 September 2021

Abstract

The mechanical properties and applications of magnetorheological elastomer films strengthened by NdFeB particles (NMRE) were investigated in this work. The NMRE film exhibited anisotropic magnetism and diverse magnetic controllability because of its large remanence and coercivity. The NMRE film was magnetized perpendicular to the surface and possessed a unique residue magnetic field. The edge of the NMRE film performed a relatively strong magnetic field, which can reach 9–10 mT, while the magnetic field in center was only 2–3 mT. This magnetic unevenness showed huge influences on the deformation of the NMRE film. When the NMRE film with fixed edge was close to a magnet, the center of the NMRE film was attracted by the magnet more observably even though the resultant force on the NMRE film was repulsive force. Based on the above unconventional deformation principle, the NMRE sound absorbers with magnetic direction-dependent tunability range were developed. The peak sound absorption frequency of NMRE sound absorbers shifted 880 Hz under an opposite magnetic field and 230 Hz under a magnetic field with the same direction. Therefore, the NMRE sound absorbers exhibit multi-level tunability and the NMRE is of great potential in complex magnetic control.

Keywords: magnetorheological elastomer, hard magnetic particles, magnetic field distribution, unconventional deformation, sound absorption

(Some figures may appear in colour only in the online journal)

1. Introduction

Magnetorheological (MR) material is a kind of smart materials, whose mechanical properties can be controlled by applying an external magnetic field [1–3]. The soft magnetic MR materials have been further composited with different functional particles to prepare magnetically sensitive materials and their physical properties such as electrical conductivity [4], thermal conductivity [5] and electromagnetic shielding [6], were controlled with a magnetic field. As a result, the MR materials showed wide application in vibration control [7–10], magnetic sensing [11], magnetic controlled movement [12, 13] and robot manufacturing [14–16].

The hard magnetic MR materials composed of hard magnetic particles in soft polymer matrix often possessed large remanence and coercivity [17–19]. In comparison to the traditional soft magnetic MR materials, more complex anisotropy of microstructure [20–22] and magnetic field distribution were presented in the hard MR materials, which provided diverse approaches for active control [23, 24]. Recently, the hard magnetic MR materials received increasing interests in magnetic drive area and various hard magnetic actuators provided diverse magnetic controllability have been developed [25, 26].

* Authors to whom any correspondence should be addressed.

Ze *et al* reported a shape-programmable magnetic material which consisted of both hard and soft magnetic particles. The matrix could be heated to soften by an alternating magnetic field and driven to deform by a constant magnetic field. The reversible controllable locked shape showed high potential in soft robotic grippers, sequential actuation devices and digital logic circuits [27]. Moreover, Deng *et al* reported a laser rewritable magnetic composite film whose magnetization direction could be rewritable when heated by laser. The rewritable magnetic composite film simplified the production process of magnetic materials and promised a wide prospect of reprogramming magnetic materials [28].

Sound absorption is a critical issue in the aerospace field and the social life [29, 30]. The film sound absorber is a widely used sound absorption structure with thin thickness, high sound absorption coefficients and single natural frequency [31, 32]. A typical film sound absorber is composed of a single film and an air cavity behind it. The film sound absorber mainly relies on the vibration and deformation of the film to convert the sound energy to the internal energy. To this end, the MR materials showed high potential in sound absorption due to their excellent flexibility, easy deformability and contactless magnetic actuation [33–35]. Based on the above analysis, it can be found that the MR elastomers with hard magnetic particles exhibited unique tunable mechanical properties under different magnetic fields. Obviously, the magnetic field distribution and its deformation mechanism in hard magnetic materials are the fundamental for applying this kind of wonderful materials in sound absorption. Therefore, developing high performance hard magnetic MR film and investigating the hard magnetic active deformation mechanism in tunable sound absorption are pressing needed.

In this work, an MR elastomer composed of NdFeB particles in silicone rubber (NMRE) was reported for high performance sound absorber. The magnetic anisotropy and the magnetic-field-induced deformation of the NMRE film were systematically investigated. Under applying a magnetic field, the NMRE films showed unconventional deformation, of which the center of the NMRE film would be attracted while the whole NMRE film was repelled by the external magnetic field. Finally, the NMRE sound absorbers were prepared and the sound absorption properties were tested under different magnetic fields. The NMRE sound absorbers performed different tunability under magnetic fields in different directions. Therefore, the NMRE sound absorbers are expected to be a particularly promising alternative for magnetic controlled movement and active sound absorption.

2. Experiment

2.1. Materials

The unmagnetized NdFeB particles were brought from Guangzhou Nuode Transmission Parts Co., Ltd, China and the average size of NdFeB particles is 5 μm. The silicone rubber Ecoflex 00-30 was purchased from Smooth-On, Inc., America.

2.2. Preparation of the NMRE film and NMRE sound absorbers

To fabricate the elastomer matrix, part A and part B of commercial silicone solution (Ecoflex 00-30) were mixed at a volume ratio of 1:1 at room temperature. Then the resulted solution was mixed with the NdFeB particles. The mass fractions of NdFeB particles were 20%, 30%, 40%, 50%, respectively. After that, the final mixture was poured into a mold (50 mm in width and length, 1 mm in height) and cured in a 1100 mT magnetic flux density for 20 min to prepared the NMRE film (figure 1). The NdFeB particles in the NMRE film were magnetized and forced to form column-like structures parallel to the direction of the magnetic field. The NMRE film also had its own magnetic poles and could interact with magnets following the law of the interaction of magnetic poles.

The NMRE film used in the sound absorbers was very thin. Therefore, the final mixture was poured on the rotor of a spin coater. The rotor rotated at 1000 rpm for 1 min and the mixture was homogenized to be a film whose thickness was about 100 μm. Then, the film was cured at 100 °C for 10 min under a small magnetic field. The small magnetic field forced the NdFeB particles to form column-like structures and kept the film surface smooth simultaneously. Finally, the cured film was exposed to a 1100 m T magnetic field for 20 min to be magnetized mostly as shown in figure 1. The magnetized film was stripped off and fixed on a frame.

2.3. Characterization of the NMRE film and NMRE sound absorbers

The magnetic properties of the NdFeB particles were measured by Hysteresis Measurement of Soft and Hard Magnetic Materials (HyMDC Metis, Leuven, Belgium). The dynamic mechanical tests of the NMRE film were carried out by the commercial rheometer (Physica MCR 302, Anton Paar Co., Austria) under the shear rate and amplitude of 1 Hz and 0.1% at room temperature. The NMRE film was prepared to be 10 mm in radius and 1 mm in thickness in the testing progress. The x-ray CT was carried out by the x-ray detection system (Dage Quadra 7, Nordson Corporation, USA). The sound absorption properties of the NMRE sound absorbers were investigated by an acoustic test system (Beijing BSWA Technology Co., Ltd, China). The sound absorption coefficient was measured by the transfer function method within the frequency range of 800–6300 Hz in compliance with the technical standards GB/T-18696.2-2002. Photos of the acoustic impedance tube (figure 2(a)) and schematic diagram of the NMRE sound absorber (figure 2(b)) were displayed in figure 2.

3. Result and discussion

3.1. Structure and magnetic properties characterizations of the NMRE film

The optical microscope photos and SEM images of different NMREs were shown in figures 3(a) and (b). The NMRE film was 1 mm in thickness and the surface of NMRE

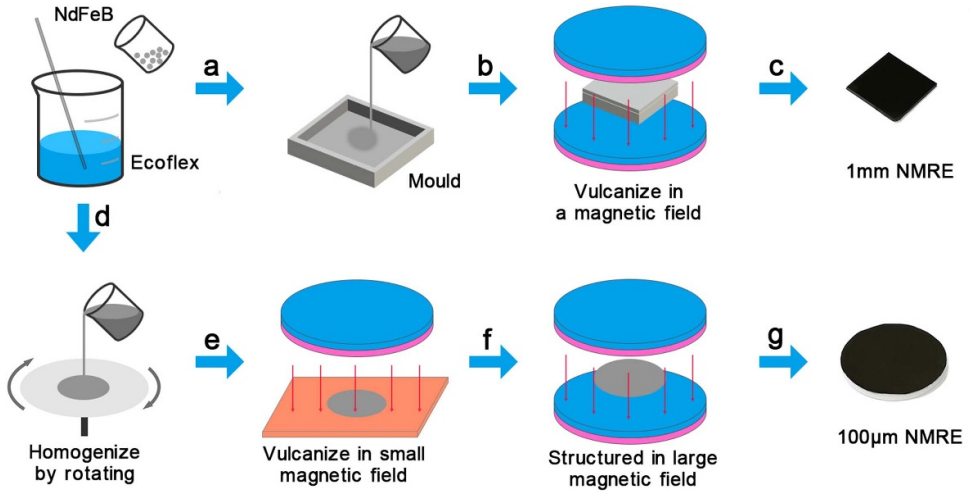

Figure 1. Schematic diagram of the material preparation process: the 1 mm NMRE film was prepared in step (a)–(c) and the 100 μm was prepared in step (d)–(g).

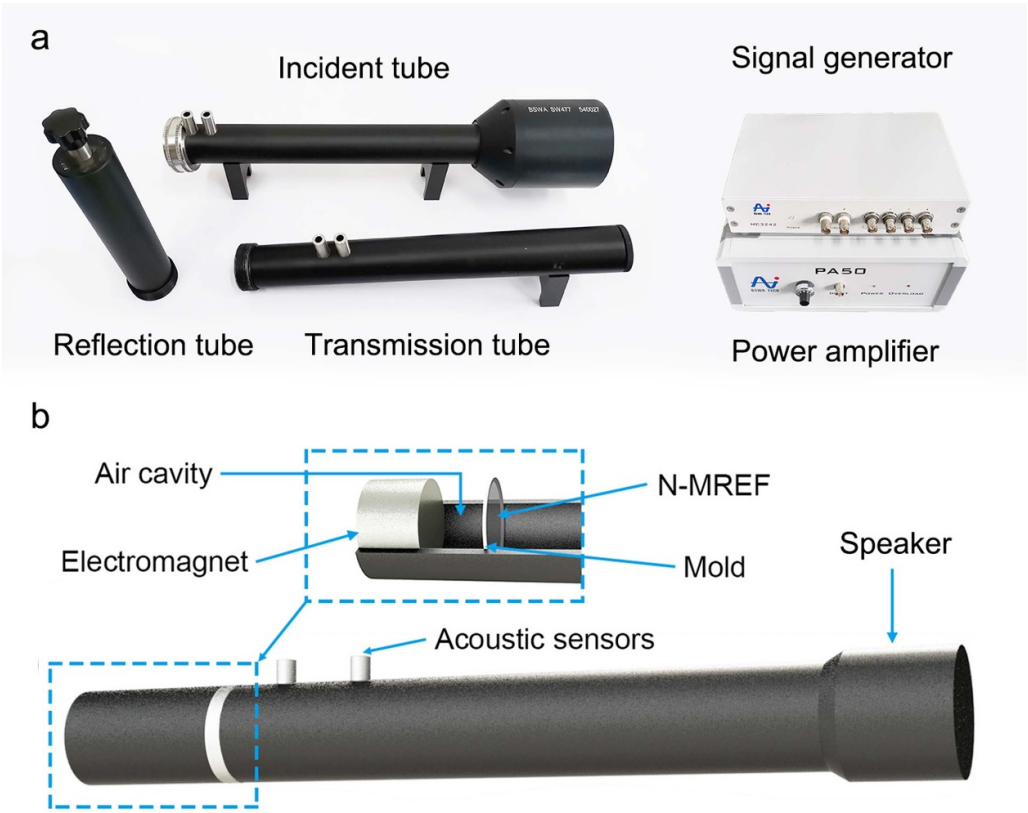

Figure 2. Photos of the acoustic impedance tube (a) and schematic diagram of the NMRE sound absorber in the acoustic impedance tube (b).

film was smooth. The NdFeB particles were irregular granular and arranged to be column-like structures in the matrix (figure 3(a)). The column-like structures were perpendicular to the film surface and tightly arranged. Figure 3(c) displayed the hysteresis loops of the NMRE film with different mass fractions. The saturated magnetization was proportional to the mass fractions of the NMRE film and the max magnetization of the 50 wt% NMRE film was 68 emu g^{-1}.

Then, the magnetic field distributions of the NMRE films were investigated as shown in figures 3(d)–(f). The original NMRE film was a square film (figure 3(d)) and its outward magnetic field was not uniform. The magnetic flux density of the film edge could reach 9–10 mT, while the magnetic flux density of the film center was only 2–3 mT. In order to further verify the magnetic field distribution of NMRE films, the original square film was cut into two parts, the round part

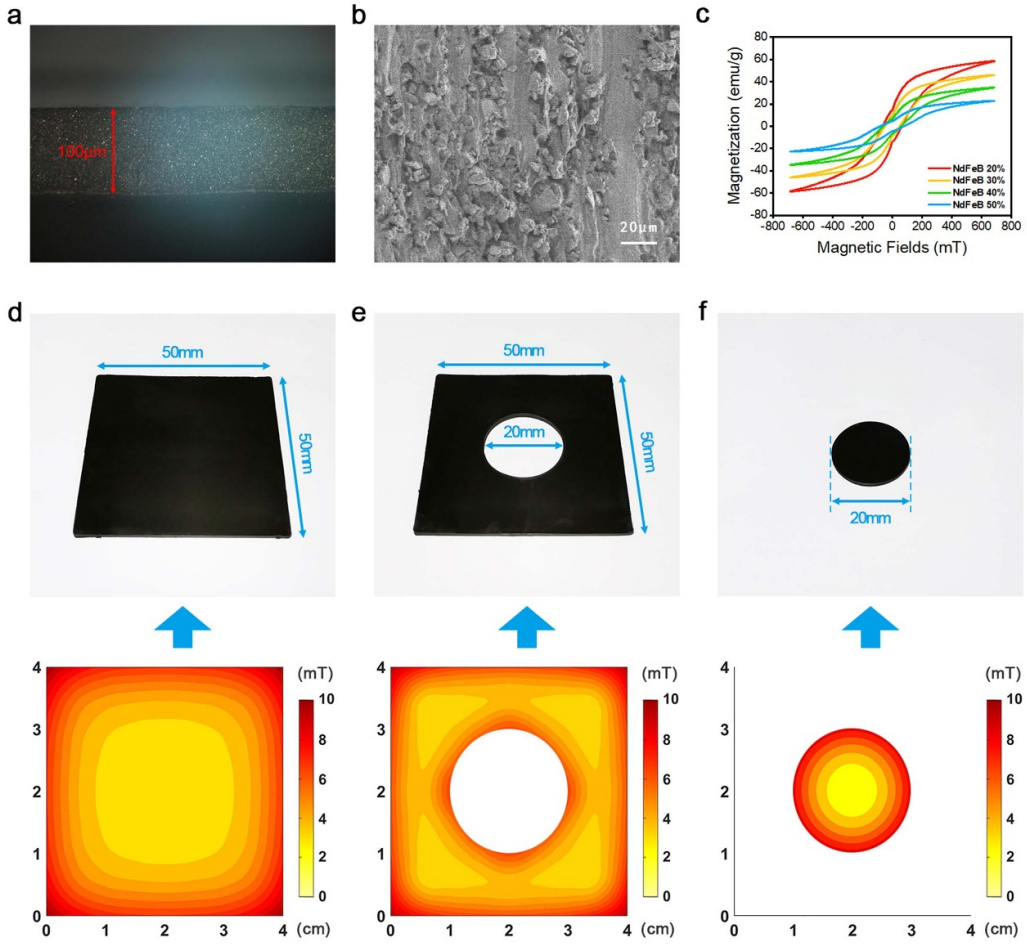

Figure 3. Optical microscope image (a), SEM image (b) and the hysteresis loops (c) of the NMRE film, the magnetic field distributions of the square film (d), irregular film (e) and round film (f).

(figure 3(f)) and remaining irregular part (figure 3(e)). These two parts both formed new outward magnetic field and followed the magnetic field distribution rule. The edge of the film performed a stronger magnetic field and the center was smaller.

The inhomogeneity of the magnetic field was significantly related to the mutual influence between adjacent magnetic dipoles. The radius of the NMRE film in this work was much larger than its height, therefore the magnetic field distribution of the NMRE film can be approximated as a two-dimensional problem. The magnetic dipoles were usually equivalent to an annular current when discussing their influence to each other (figure 4(a)). At first, the magnetic dipoles distributed chaotically in the matrix. Under ideal conditions, the magnetization was assumed to be uniform. The magnetic dipoles would be all readjusted to be parallel to the direction of the external magnetic field (figure 4(b)). Then, the magnetic dipoles were equivalent to annular currents in figure 4(c). In the middle area of the film, the magnetic flux density was small because the contribution of every magnetic dipole was partially offset by the nearest magnetic dipoles. The current directions of the adjacent magnetic dipoles were antiparallel. In contrast, the magnetic dipoles at the edge of the film received less influence from fewer near magnetic dipoles. Therefore, the magnetic flux density was stronger at the edge of the film. When the NMRE film was cut into two parts, the magnetic field distribution cannot remain unchanged. The magnetic fields would redistribute following the electromagnetic equivalent principle above and formed strong magnetic field at the edge of the film.

3.2. Mechanical properties of the NMRE film

At first, the magnetic flux density scanning tests were carried out by the commercial rheometer. Two faces of the NMRE film performed different MR properties because the NMRE film formed its own magnetic poles and had different interactions to different magnetic fields. The direction of the magnetic field in the rheometer was kept upright throughout the experiment. The MR properties of NMRE films were measured with the S pole and the N pole upward in turn. When the N pole was upward, the magnetic directions of the NMRE film and the rheometer were the same. As shown in figure 5(a), the storage modulus of the NMRE film increased gradually with the magnetic flux density and there was no obvious magnetic saturation process. The NMRE film had low initial modulus and easy deformability. The 50 wt% NMRE film got the highest storage modulus, which reached to 113 kPa under a 1000 mT magnetic flux density. Differently, when the S pole

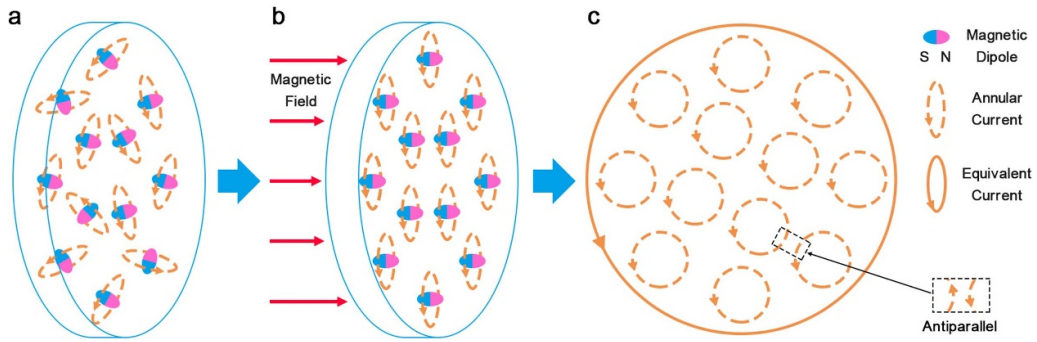

Figure 4. Mechanism explanation of the magnetic field distribution: chaotic distribution (a), regular distribution under a magnetic field (b) and the schematic diagram of equivalent current (c).

was upward, the storage modulus decreased sharply with the magnetic field at first and increased slowly after the magnetic flux density was over 500 mT (figure 5(b)). Different magnetic field loading directions were equivalent to loading from different points in the hysteresis loops. When the NMRE's magnetic field and the external magnetic field were in the same direction, this situation was equivalent to loading from point *P* on the hysteresis loops (figure 5(c)). The magnetization of NMRE was strengthened and the modulus increased. On the contrary, when the NMRE was exposed to an opposite magnetic field, it was equivalent to loading from point *Q* on the hysteresis loops (figure 5(d)). The magnetization of NMRE decreased at first and then increased in the opposite direction, which was consistent with the variation trend of the modulus. Different with the soft magnetic MREs whose magnetic properties were isotropic, the NMRE film performed a completely different MR properties under magnetic fields in different directions. This was the most important advantage of hard magnetic MREs. As shown in figure 6(a), the direction of the magnetic field also played an important influence on the loss modulus.

Then, the shear strain scanning tests and the creep tests under different magnetic fields were conducted on the 50 wt% NMRE film. The NMRE film showed an obvious Payne effect, in which the storage modulus decreased sharply with the increasing of shear strain. Magnetic fields in different directions also had different influence on the strain dependent mechanical properties. An opposite magnetic field decreased the storage modulus of NMRE films, while a magnetic field in the same direction enhanced the storage modulus (figure 6(b)). In the creep tests, the shear strain tended to be stable rapidly when a 1500 Pa shear stress was applied and decreased sharply to zero after the stress was removed. In the meantime, the directions of the magnetic field also had opposite influence on the creep curves. The shear strain increased under an opposite magnetic field, while shear strain decreased if the NMRE film exposed in a same direction magnetic field (figure 6(c)).

However, the NMRE film cannot maintain its magnetic field under extreme conditions. The magnetic field of the NMRE film would be undermined if exposed to a large opposite magnetic field for a long time. Figure 6(d) displayed the storage modulus curves under an opposite magnetic field after processed by ladder magnetic fields. An opposite magnetic flux density stronger than 500 mT weakened the magnetism of the NMRE film and decreased its MR effect. This phenomenon was because that not all the NdFeB particles in NMRE films were completely magnetized during the preparation process. When the NMRE film was exposed to a large opposite magnetic field, the unmagnetized NdFeB particles in the NMRE film were magnetized in an opposite direction, thus the magnetism of the NMRE film became more chaotic and its magnetic control performance was decreased. The magnetism of the NMRE film would tend to be stable after the 1000 mT magnetic field was loaded for five times.

3.3. *Deformation of the NMRE film under a magnetic field*

To investigate the deformation of the NMRE film, the interaction between the NMRE film and the magnet was detailly investigated. The NMRE film had its own magnetic poles and could interact with magnets following the law of interaction between magnetic poles. When the center of the NMRE film was fixed, the edge deformed due to the magnetic field induced forces. The NMRE film and the magnet repelled each other when the same magnetic poles were face to face. On the contrary, they attracted each other when the opposite magnetic poles were approached (figure 7(c)). However, the phenomenon was significantly different when the edge of the NMRE film was fixed. Figures 7(a) and (b) showed clearly that the NMRE film and the magnet attracted each other whether any two poles were face to face or not. Interestingly, the center of the NMRE film was attracted by the magnet more obviously when the resultant force was repulsive force (figure 7(a)). This phenomenon was significantly related to the magnetic field distributions of the NMRE film.

In this case, the NMRE film cannot be simplified to a mass point and different parts of the NMRE film received different forces. Therefore, the NMRE film was divided into two imaginary parts, the strong magnetic region at the edge and the weak magnetic region at the center (figure 7(e)). The strong magnetic region at the edge had its own magnetic poles and could interact with magnets normally. The weak magnetic region at the center could not perform the repulsive force because of its low magnetism. The NdFeB particles in the NMRE would always be magnetized provisionally and the NMRE was attracted by the external magnetic field regardless of the direction of the magnetic field. Figures 7(f) and

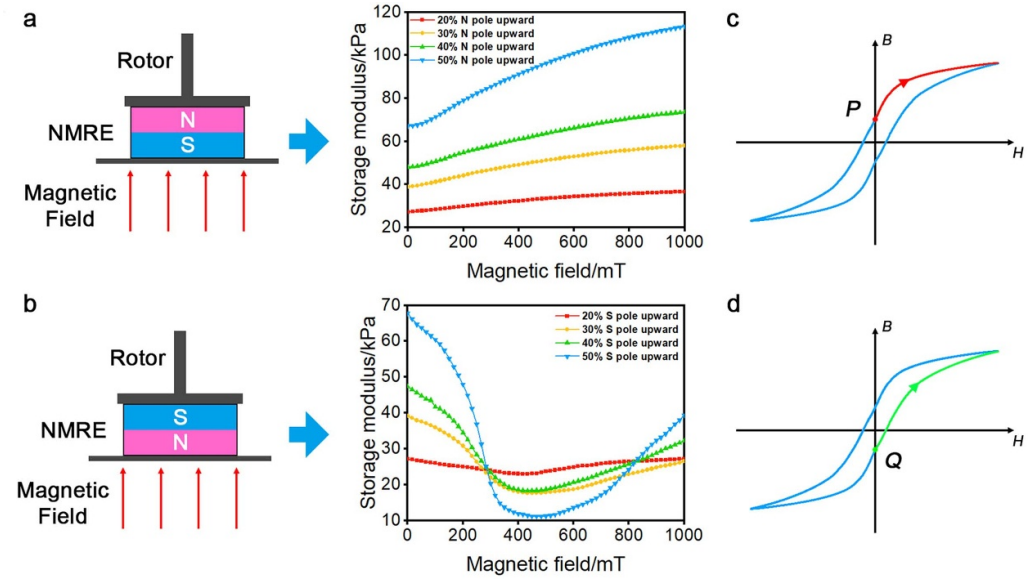

Figure 5. Storage modulus with the N pole upward (a) and the S pole (b) upward and their schematic testing diagram, mechanical mechanism of two kinds of loading directions (c), (d).

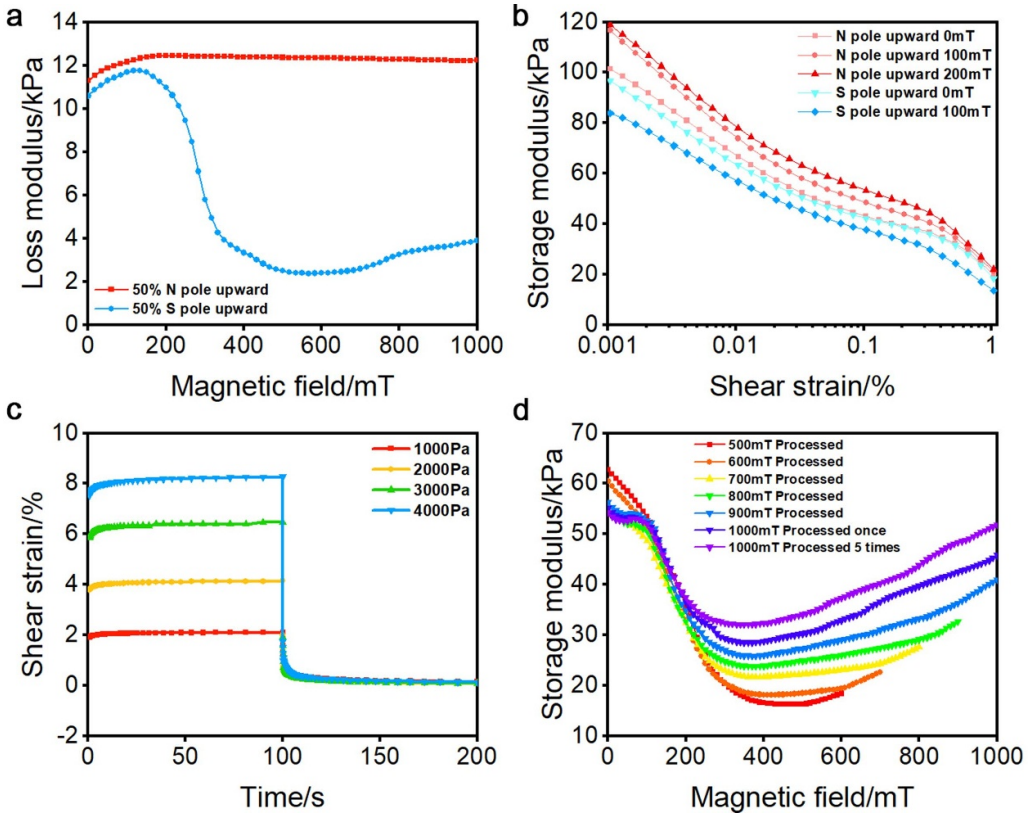

Figure 6. Loss modulus (a), shear strain scanning (b) under different magnetic field, creep tests under different shear stress (c), repeated magnetic field loading tests (d).

(g) shows the received forces of the NMRE film under different magnetic field. When the external magnetic field was opposite to the magnetic field of NMRE film, the NMRE film was subjected to a torque and easier to be deformed out-of-plane (figure 7(f)). On the contrary, the NMRE film was subjected to a uniform force under a magnetic field in the same direction, thus the out-of-plane displacement was difficult to be achieved (figure 7(g)). In order to verify this explanation, the weak magnetic region at the center of the NMRE film was cropped. As shown in figure 7(d), the cropped region and the remaining region would redistribute the outward magnetic field and repeal each other. Typically, the cropped region could

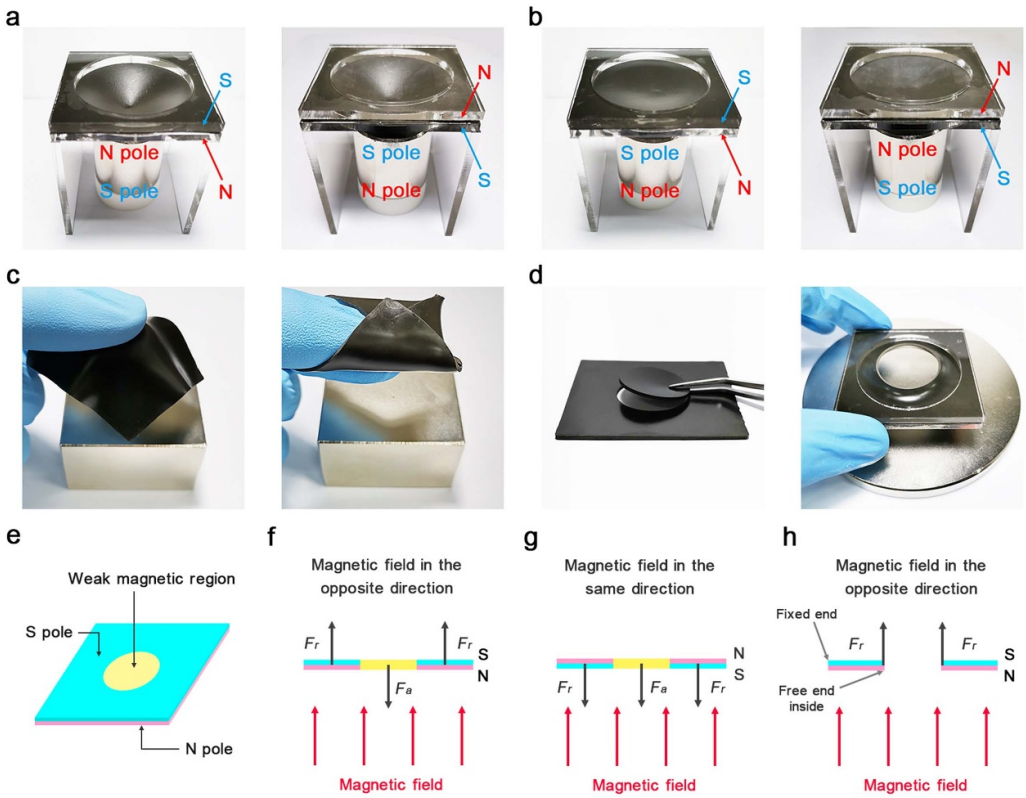

Figure 7. Deformations of the NMRE film under magnetic fields in opposite directions (a) and same directions (b) with the edge fixed, deformations of the NMRE film with the center fixed (c), interaction and deformation after the NMRE film was cut into two parts (d), and the area division (e) and force analysis (f)–(h) of NMRE films.

not be put back to the original position. Figure 7(d) shows the deformation of the remaining region which was exposed to a magnetic field with same magnetic poles. Interestingly, different from the intact NMRE, the middle part of the tailoring film and the magnet no longer attracted each other. The middle part of the film was repelled by the magnet and shaped like an umbrella. This was because that the middle part of the film changed to be a strong magnetic region after cutting the center of the film. The strong magnetic region should interact with magnets normally and repel the magnet with a same magnetic pole.

Then the deformation of the thin NMRE film was measured. This kind of NMRE film was 100 μm in thickness and easier to deform. This thickness ensures that the natural frequency of the sound absorber fell within the frequency range of the acoustic test. Figures 8(a) and (b) displayed the deformations of the NMRE film under the magnetic fields with different strengths and directions. The out-of-plane displacement showed positive correlation with the magnetic flux density. The max out-of-plane displacement reached 8.1 mm when a 300 mT opposite magnetic field was applied to the film.

Furthermore, the microstructure of the NMRE film was investigated when the film was deformed. An x-ray computed tomography system was employed to detect the 3D image of the NdFeB particles in the matrix. Figure 8(c) showed the CT image of the 50% NMRE film in its original state. The NdFeB particles were arranged to form column-like structures orderly in the matrix. When the NMRE film was driven to deform, the directions of column-like structures would turn with the matrix and rearrange in a sector. The radius of curvature in this test was 5.17 mm, which was correspond with the deformation of the thin NMRE film under a 300 mT opposite magnetic field (figure 8(d)). The deformation would not destroy the column-like structures in the matrix and the column-like structures would restore to the original arrangement when the external force was removed.

3.4. Sound absorption of the NMRE sound absorber

When a sound wave encountered a wall or other obstacle, part of the sound energy was reflected, part of the sound energy was absorbed by the wall or obstacle and converted into heat energy, and the other part of the sound energy was transmitted to the other side. The reflected energy was a critical parameter for sound absorption and less reflected energy meant better sound absorption properties.

The NMRE sound absorber was composed of an NMRE film and the air cavity behind it. The NMRE film and the air cavity formed a resonant structure together. The sound absorption coefficient reached the maximum value when the frequency of incident sound wave was close to the natural frequency of the sound absorption structure. Therefore, the typical sound absorption curve of the NMRE sound absorber was unimodal in the measured frequency range (figures 9(a)–(d)).

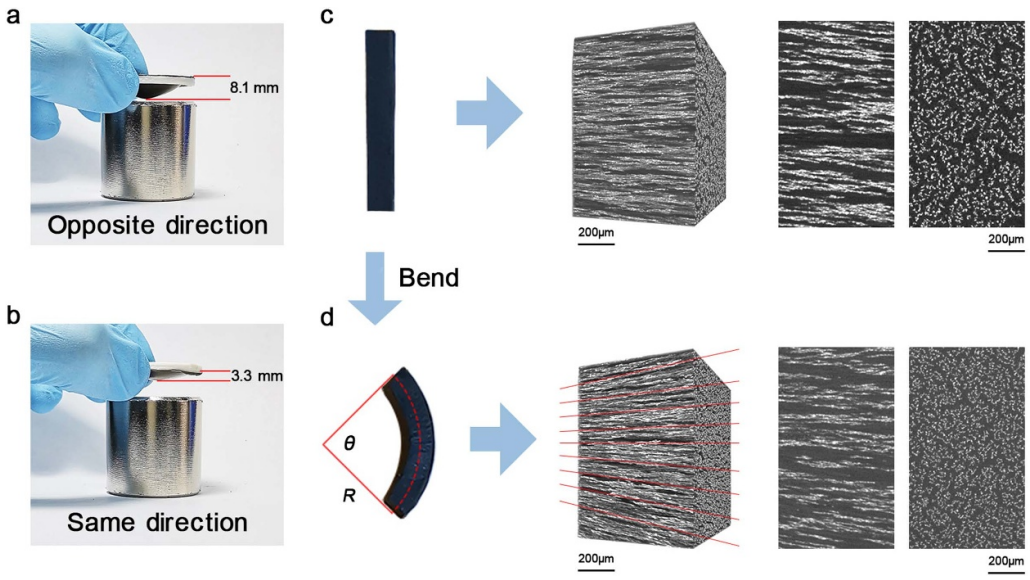

Figure 8. Deformations of the thin NMRE film under magnetic fields in different directions (a), testing device and x-ray CT image for the original NMRE film (c) and the crooked NMRE film (d).

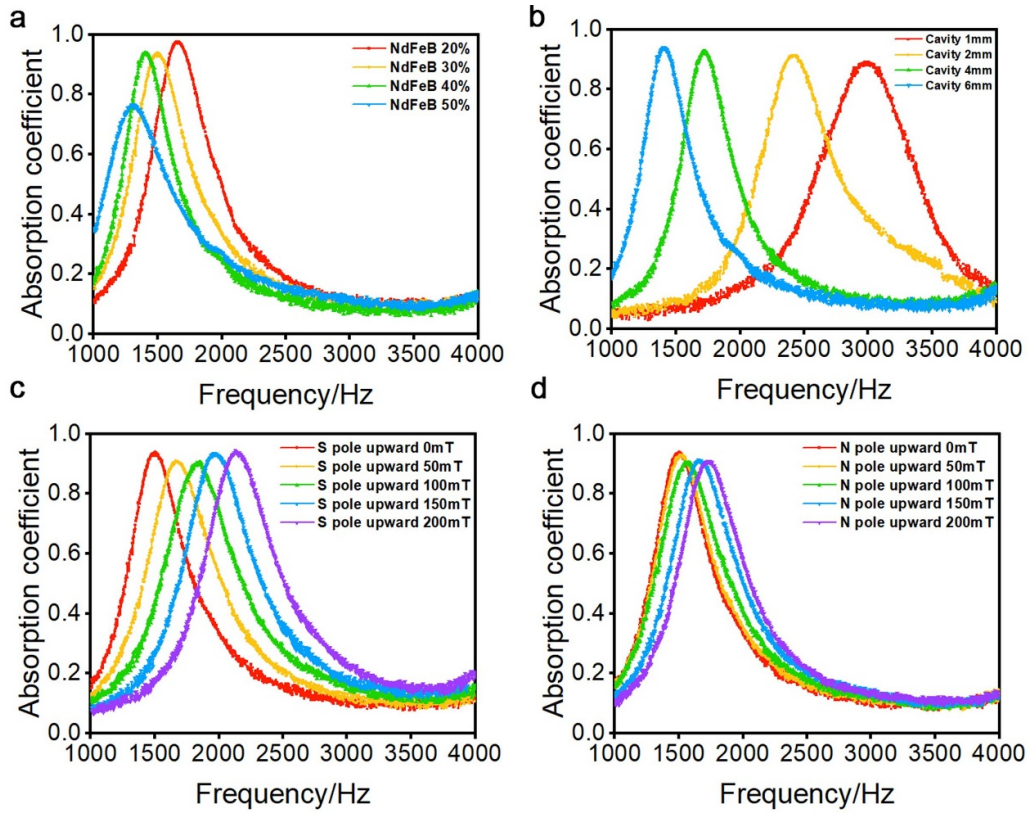

Figure 9. The influences of the mass fractions of NdFeB particles (a), air cavity length (b) and magnetic flux density (c), (d) on the sound absorption curves.

The structural parameters of the NMRE sound absorber, including the mass fractions of NMRE films and air cavity length, exhibited important influence on the peak sound absorption frequency. A higher mass fraction of NdFeB particles would shift the peak sound absorption frequency to a low frequency range and the sound absorption coefficient decreased from 0.97 to 0.76 simultaneously (figure 9(a)). Higher mass fractions increased the surface density of the NMRE film and the natural frequency shifted to a lower frequency. The NMRE film with high mass fractions also became harder and more difficult to be vibrated. In this case, less sound energy was consumed by vibration, thus the sound absorption coefficient decreased.

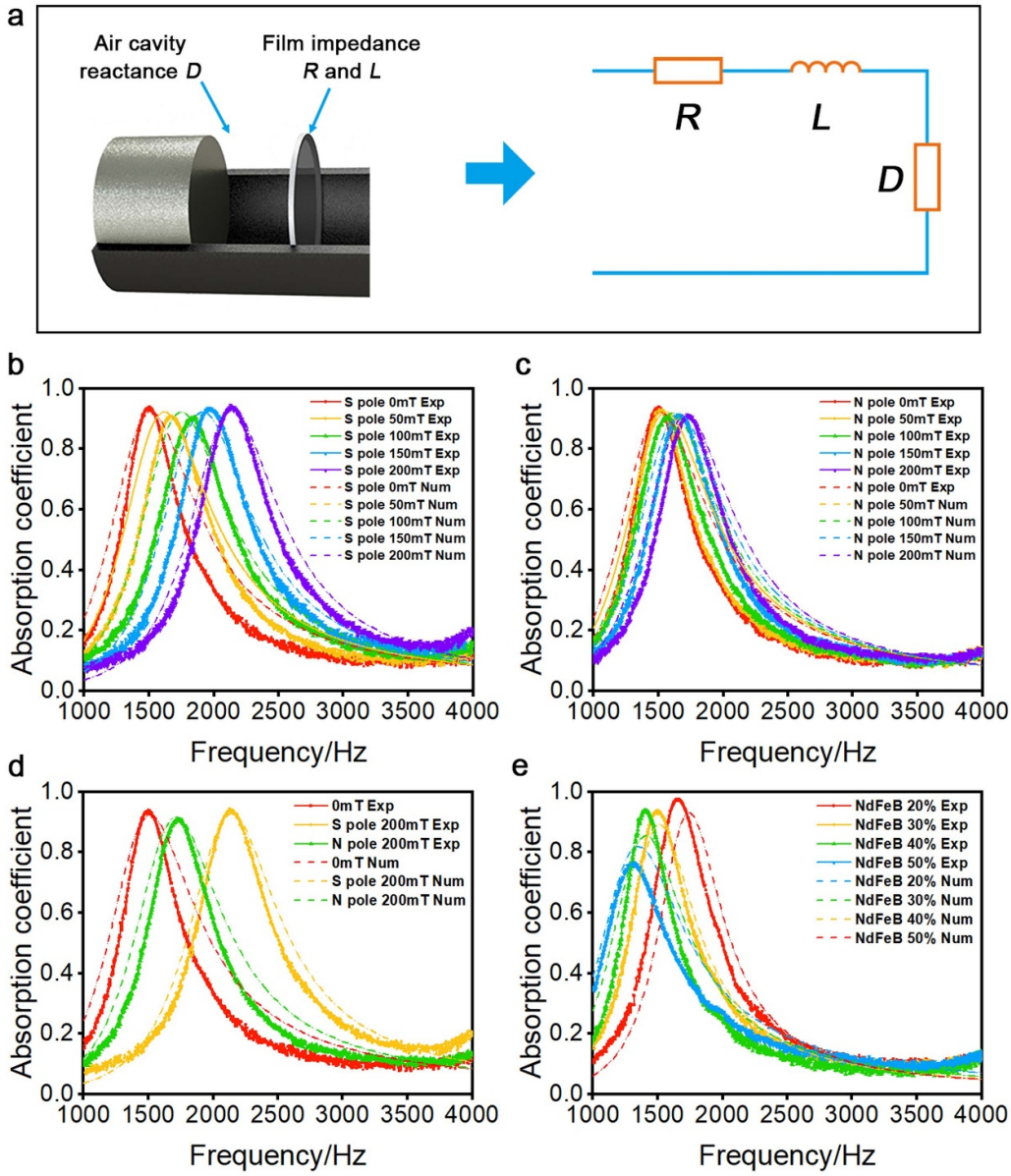

Figure 10. Schematic diagram of the NMRE sound absorber and the equivalent circuit (a), comparisons between experimental data and numerical results of magnetic flux density (b)–(d), mass fractions (e).

The air cavity length was a more efficient mean to adjust the sound absorption curves and it could shift the peak sound absorption frequency in a wide frequency range without decreasing the sound absorption coefficient (figure 9(b)). The air cavity length can tune the natural frequency of the NMRE sound absorber but had no negative effect on the vibration of NMRE film. However, the air cavity length was unchangeable once the NMRE sound absorber was manufactured. The MR effect provided another way to adjust the peak sound absorption frequency by the magnetic field as shown in figures 9(c) and (d). The NMRE film deformed under different magnetic fields and the air cavity length changed accordingly. As a result, the peak sound absorption frequency was tunable by the magnetic fields. Furthermore, the NMRE film had different reactions to the directions of magnetic fields. An opposite magnetic field could deform the NMRE film significantly and tune the peak sound absorption frequency in a wide frequency range. The peak sound absorption frequency shifted from 2380 Hz to 1500 Hz under a 200 mT magnetic field (figure 9(c)). Oppositely, a magnetic field in the same direction with the NMRE film could deform the NMRE film slightly and tune the peak sound absorption frequency more subtly, of which the peak sound absorption frequency was shifted by 230 Hz (figure 9(d)).

3.5. Numerical solutions for sound absorption curves

In order to further understand the sound absorption performance of the sound absorption structure, an equivalent circuit method was employed to predict the sound absorption curves [36, 37]. The equivalent circuit was displayed in figure 10(a), in which R and L represented the acoustic resistance and

reactance of the components, D was the air cavity length. The components in the circuit were connected in series. Then the sound absorption coefficient could be calculated by a classic formula:

$$\alpha = \frac{4Re\,(z)}{[1+Re\,(z)]^2+[Im\,(z)]^2} \tag{1}$$

where z is the normalized specific acoustic impedance of the equivalent circuit and it consists of two parts, the acoustic impedance of the film z_m (2) and the acoustic impedance of the air cavity z_c (3):

$$z_m = \frac{R+jL}{\rho c} = r + j\omega m \tag{2}$$

$$z_c = -j\cot\frac{\omega D}{c} \tag{3}$$

where ρ is the density of air, c is the sound velocity in air, ω is the angular frequency and $\omega = 2\pi f$, f is the frequency, m is the surface density of the NMRE film, D is the length of the air cavity, d is the thickness of the membrane, r is the normalized specific sound resistance of the NMRE film, r is related to the installation conditions and $r = 80.42df^{1/2}$ here [36]. According to the equivalent circuit diagram in figure 10(a), the normalized specific acoustic impedance z can then be calculated as follows:

$$z = z_m + z_c = r + j\left(\omega m - \cot\frac{\omega D}{c}\right). \tag{4}$$

Then, the final expression of the sound absorption coefficient can be expressed as:

$$\alpha = \frac{4r}{[1+r]^2+\left[\omega m - \cot\frac{\omega D}{c}\right]^2}. \tag{5}$$

The sound absorption coefficient reaches the maximum value when $\omega m = \cot\left(\frac{\omega D}{c}\right)$ and the maximum absorption coefficient is:

$$\alpha_{\max} = \frac{4r}{[1+r]^2}. \tag{6}$$

The numerical solutions for sound absorption coefficients were calculated as shown in figures 10(b)–(e). The solid curves and the dash dot curves represented the experiment results and the numerical results respectively. The numerical solutions for mass fractions of NdFeB particles matched well with the experiments (figure 10(e)). Figures 10(b) and (c) displayed the influence of different magnetic fields on the sound absorption curves. The intuitive comparison of magnetic fields in different directions was showed in figure 10(d). Different directions of magnetic fields had different tunability, which was consistent with experimental results. The deformations caused by magnetic fields changed the tension on the NMRE film and the air cavity length, which determined the acoustic resistance of the NMRE film and the acoustic impedance of the air cavity, respectively. Among them, the acoustic impedance of the air cavity played a dominant role and the decreased air cavity length shifted the peak sound absorption frequency to the high frequency range.

Therefore, the performance of the NMRE sound absorbers was tunable by varying the magnetic fields with different directions. An opposite magnetic field showed a rough tunability on the peak sound absorption frequency, while a same direction magnetic field tuned the peak sound absorption frequency subtly. Based on the above analysis, it can be concluded that the NMRE sound absorbers provided diversified tunability in the field of acoustic active control.

4. Conclusion

This work reported the NdFeB based hard magnetic MRE films which exhibited anisotropic magnetism and diverse magnetic controllability. The magnetic field distribution and the magnetic induced deformation of the NMRE film were detailly investigated. The NMRE film performed a larger magnetic field at the edge and a smaller magnetic field in the center whatever the shape of the film was. The interaction between the NMRE film and the magnetic field became complicated because of the magnetic anisotropy. The NMRE film was divided into two imaginary parts, the strong magnetic region at the edge and the weak magnetic region at the center. Therefore, the magnet attracted the NMRE film whether any two poles faced to face when the edge of the NMRE film was fixed. The NMRE sound absorbers with different tunability were prepared based on this unconventional deformation characteristic. The NMRE sound absorbers had excellent sound absorption properties near the natural frequency. The magnetic field can shift the peak sound absorption frequency by changing the tension on the NMRE film and the air cavity length. An opposite magnetic field could deform the NMRE film significantly and tune the peak sound absorption frequency in a wide frequency range. Oppositely, a magnetic field in the same direction with the NMRE film could deform the NMRE film slightly and tune the peak sound absorption frequency subtly. Finally, the equivalent circuit method was employed to verify the sound absorption properties and agreed with the experimental results. Therefore, the NMRE sound absorbers performed significant and various tunability under magnetic fields in different directions. The NMRE film exhibits unconventional magnetic anisotropy and deformability, thus it possesses high potential for active control and sound absorption.

Data availability statement

The data generated and/or analyzed during the current study are not publicly available for legal/ethical reasons but are available from the corresponding author on reasonable request.

Acknowledgments

Financial supports from the National Natural Science Foundation of China (Grant Nos. 11822209, 12132016, 12072338), the Fundamental Research Funds for the Central Universities (WK2480000007, WK2480000009), Joint Fund of USTC-National Synchrotron Radiation Laboratory (KY2090000055), the Anhui's Key R&D Program of China (202104a05020009), and Strategic Priority Research Program of the Chinese Academy of Sciences (Grant No. XDB22040502) are gratefully acknowledged.

ORCID iD

Xinglong Gong https://orcid.org/0000-0001-6997-9526

References

[1] Ju B, Tang R, Zhang D, Yang B, Yu M, Liao C, Yuan X, Zhang L and Liu J 2016 Dynamic mechanical properties of magnetorheological elastomers based on polyurethane matrix *Polym. Compos.* **37** 1587–95
[2] Xu J Q, Wang P F, Pang H M, Wang Y, Wu J, Xuan S H and Gong X L 2018 The dynamic mechanical properties of magnetorheological plastomers under high strain rate *Compos. Sci. Technol.* **159** 50–58
[3] Xuan S H, Xu Y G, Liu T X and Gong X L 2015 Recent progress on the magnetorheological plastomers *Int. J. Smart Nano Mater.* **6** 135–48
[4] Ding L, Xuan S H, Pei L, Wang S, Hu T and Gong X L 2018 Stress and magnetic field bimode detection sensors based on flexible Cl/CNTs-PDMS sponges *ACS Appl. Mater. Interfaces* **10** 30774–84
[5] Ren L *et al* 2018 A liquid-metal-based magnetoactive slurry for stimuli-responsive mechanically adaptive electrodes *Adv. Mater.* **30** 1802595
[6] Sang M, Wu Y X, Liu S, Bai L F, Xuan S H and Gong X L 2021 Flexible and lightweight melamine sponge/MXene/polyborosiloxane (MSMP) hybrid structure for high-performance electromagnetic interference shielding and anti-impact safe-guarding *Composites* B **211** 108669
[7] Fu J, Li P, Wang Y, Liao G and Yu M 2016 Model-free fuzzy control of a magnetorheological elastomer vibration isolation system: analysis and experimental evaluation *Smart Mater. Struct.* **25** 035030
[8] Liu X, Wang N, Wang K, Huang H and Li W H 2019 Optimizing vibration attenuation performance of a magnetorheological damper-based semi-active seat suspension using artificial intelligence *Front. Mater.* **6** 269
[9] Zhang Y, Fang F, Huang W, Chen Y and Yu M 2019 Dynamic mechanical hysteresis of magnetorheological elastomers subjected to the cyclic loading and periodic magnetic field *Front. Mater.* **6** 292
[10] Acharya S, Allien V J, Puneet N P and Kumar H 2021 Dynamic behavior of sandwich beams with different compositions of magnetorheological fluid core *Int. J. Smart Nano Mater.* **12** 88–103
[11] Hu T, Xuan S H, Ding L and Gong X L 2020 Liquid metal circuit based magnetoresistive strain sensor with discriminating magnetic and mechanical sensitivity *Sens. Actuators* B **314** 128095
[12] Lum G Z, Ye Z, Dong X, Marvi H, Erin O, Hu W and Sitti M 2016 Shape-programmable magnetic soft matter *Proc. Natl Acad. Sci. USA* **113** 6007–15
[13] Chen S, Li R, Li X and Wang X 2018 Magnetic field induced surface micro-deformation of magnetorheological elastomers for roughness control *Front. Mater.* **5** 76
[14] Eric D, Jiang Z, Guo Z L, Matthew R E and Metin S 2014 Continuously distributed magnetization profile for millimeter-scale elastomeric undulatory swimming *Appl. Phys. Lett.* **104** 174101
[15] Feng J B, Xuan S H, Ding L and Gong X L 2017 Magnetoactive elastomer/PVDF composite film based magnetically controllable actuator with real-time deformation feedback property *Composites* A **103** 25–34
[16] Vien Q N, Duy T L, Dai H L, Nguyen Q H and Choi S B 2019 Material characterization of MR fluid on performance of MRF based braker *Front. Mater.* **6** 125
[17] Kim M W, Han W J, Kim Y H and Choi H J 2016 Effect of a hard magnetic particle additive on rheological characteristics of microspherical carbonyl iron-based magnetorheological fluid *Colloids Surf.* A **506** 812–20
[18] Wen Q Q, Wang Y and Gong X L 2017 The magnetic field dependent dynamic properties of magnetorheological elastomers based on hard magnetic particles *Smart Mater. Struct.* **26** 075012
[19] Xie Y, Qi S, Fu J, Tian R, Liu F and Yu M 2021 A pre-magnetized NdFeB-particle reinforced magnetorheological elastomer *Smart Mater. Struct.* **30** 014002
[20] Pallapa M and Yeow J T W 2015 A review of the hybrid techniques for the fabrication of hard magnetic microactuators based on bonded magnetic powders *Smart Mater. Struct.* **24** 025007
[21] Schümann M, Borin D Y, Huang S, Auernhammer G K, Müller R and Odenbach S 2017 A characterisation of the magnetically induced movement of NdFeB-particles in magnetorheological elastomers *Smart Mater. Struct.* **26** 095018
[22] Zhao R, Kim Y, Chester S A, Sharma P and Zhao X 2019 Mechanics of hard-magnetic soft materials *J. Mech. Phys. Solids* **124** 244–63
[23] Kim Y, Yuk H, Zhao R, Chester S A and Zhao X 2018 Printing ferromagnetic domains for untethered fast-transforming soft materials *Nature* **588** 274–9
[24] Liu A C, Gillen J H, Mishra S R, Evans B A and Tracy J B 2019 Photothermally and magnetically controlled reconfiguration of polymer composites for soft robotics *Sci. Adv.* **5** 2897
[25] Hu W, Lum G Z, Mastrangeli M and Sitti M 2018 Small-scale soft-bodied robot with multimodal locomotion *Nature* **554** 81–85
[26] Ubaidillah D P E, Hanafi I, Choi S B, Abdul A A and Amri M S 2019 Swelling, thermal, and shear properties of a waste tire rubber based magnetorheological elastomer *Front. Mater.* **6** 47
[27] Ze Q, Kuang X, Wu S, Wong J, Montgomery S M, Zhang R, Kovitz J M, Yang F, Qi H J and Zhao R 2020 Magnetic shape memory polymers with integrated multifunctional shape manipulation *Adv. Mater.* **32** 1906657
[28] Deng H, Sattari K, Xie Y, Liao P and Lin J 2020 Laser reprogramming magnetic anisotropy in soft composites for reconfigurable 3D shaping *Nat. Commun.* **11** 6325
[29] Cao X F, Xuan S H, Li J, Li J Y, Hu T, Liang H Y, Ding L, Li B S and Gong X L 2020 Magnetic-tunable sound absorber based on micro-perforated magnetorheological elastomer *Smart Mater. Struct.* **29** 015024
[30] Paolo G, Emanuele T and Dal B L 2020 Comparison of smart panels for tonal and broadband vibration and sound

transmission active control *Int. J. Smart Nano Mater.* **11** 431–84
[31] Zhao J, Li X, Wang Y, Wang W, Zhang B and Gai X 2017 Membrane acoustic metamaterial absorbers with magnetic negative stiffness *J. Acoust. Soc. Am.* **141** 840–6
[32] Gai X L, Xing T, Li X H, Zhang B, Cai Z N and Wang F 2018 Sound absorption properties of microperforated panel with membrane cell and mass blocks composite structure *Appl. Acoust.* **137** 98–107
[33] Sánchez P A, Stolbov O V, Kantorovich S S and Raikher Y L 2019 Modeling the magnetostriction effect in elastomers with magnetically soft and hard particles *Soft Matter* **15** 7145–58
[34] Stepanov G V, Borin D Y, Bakhtiiarov A V and Storozhenko P A 2019 Negative coercivity of magnetic elastomers filled with magnetically hard particles *J. Magn. Magn. Mater.* **498** 166125
[35] Schümann M, Borin D Y, Morich J and Odenbach S 2020 Reversible and non-reversible motion of NdFeB-particles in magnetorheological elastomers *J. Intell. Mater. Syst. Struct.* **32** 3–15
[36] Kang J and Fuchs H V 1999 Predicting the absorption of open weave textiles and micro-perforated membranes backed by an air space *J. Sound Vib.* **220** 905–20
[37] Soltani P and Zerrebini M 2012 The analysis of acoustical characteristics and sound absorption coefficient of woven fabrics *Text. Res. J.* **82** 875–82